Sub Topic: Fire Research

12th U. S. National Combustion Meeting
Organized by the Central States Section of the Combustion Institute
May 24–26, 2021 (Virtual)
College Station, Texas

Burning Characteristics of Small Firebrands in Wildland-Urban-Interface Fires

Byoungchul Kwon, Ya-Ting T.Liao

Department of Mechanical and Aerospace Engineering, Case Western Reserve University, Cleveland, OH 44106, USA

*Corresponding Author Email: yating.liao@case.edu

Abstract: Firebrand attack has been shown to be one of the key mechanisms of wildfire spread into Wildland-Urban Interface (WUI) communities. The ignition propensity of materials caused by firebrands depends on not only the attributes (e.g., shape, size, numbers) but also the distribution of firebrands after landing on the substrate materials. To help characterize this process, this study aims to first investigate the effects of gap spacing on the burning behaviors of a group of wooden samples. Experiments were conducted using 9 wooden cubes, 19mm-long on each side. These samples were arranged in a 3 by 3 square pattern on suspension wires. The gap spacing (s) between the cube samples varies from 0 to 30 mm. Burning process was recorded using video cameras. Sample mass loss and temperatures were monitored during the flaming and smoldering processes. The results show that when $s \le 10$ mm, flames from individual samples merged. When the gap spacing reduces, the mass loss rate first increases but starts decreasing at s = 10 mm where flame merging occurs. The flame height has a similar non-monotonic dependency on the gap spacing and the maximum flame height occurs at s = 5 mm. Compared to the case with s = 10 mm, cases with a smaller gap spacing (s = 2.5 and 5 mm) have a larger flame height but a smaller sample mass loss rate. This indicates that a reduced air entrainment leads to an increase in the flame height despite of a decreased flame heat feedback to the solid samples. The heating rates of each sample were also calculated to investigate the local burning behaviors. The analysis showed a weaker flame heat feedback to the sample at the center for cases with under-ventilated combustion. Last, gaseous flame height was corelated to the solid burning rate. The correlation was also compared with previous empirical equations concerning liquid pool fires of different heat release rates.

Keywords: group burning, firebrand ignition, wildland-urban-interface(WUI)

1. Introduction

As the climate change becomes intense, the increase in global temperature is expected to cause hotter and drier weather conditions favorable for wildfire in the future [1,2]. Especially, the year of 2020 was the second warmest since 1880 and the state of California suffered from severe wildfires, including four of top five largest fires on record [3,4]. Once a wildfire invades wildland-urban interface (WUI) region, it can cause not only structure losses but also heavy casualties, as the Camp Fire in 2018 [5].

One particular way of wildfire spread is spot ignition caused by firebrands. Small flaming or glowing embers were identified to be responsible for ignition of new vegetation or structures remote from wildfire front [6–8]. Most of firebrands have a mass less than 1 g and various sizes and shapes depending on their sources and wind conditions [8]. In experiments of burning structures typically observed in WUI, most firebrands were found to have 0.9-3.61 cm2 projected

area [9–11]. Ignition induced by firebrands is a complex process. It is highly affected by environmental conditions (e.g., wind, temperature) and thermal interactions between the brands and the recipient fuel. Previous experiments using realistic firebrand shower revealed that the accumulation or proximity between firebrands can ignite common wood structures in WUI or highly moisturized vegetation under wind conditions [12–18]. The intensified heat generation from accumulated firebrands was also experimentally confirmed by the increased heat flux from greater amount of deposited firebrands pile [19–21] and multiple number of firebrands [22,23] upon a recipient fuel. It was also found that the smaller bulk density of firebrand pile can generate higher heat flux [20]. This is because of the larger actual surface area contacting airflow which triggers more vigorous smoldering combustion on firebrand surfaces. These literatures imply the critical influence of heat source concentration along with the air supply facilitating the exothermic oxidation process on the intensity of heat generated.

Similar phenomena of heat source concentration and air supply can be found in multiple fires. Thermal interaction between multiple fires have been studied for many years since it is more realistic fire scenarios. For multiple fires, the global burning characteristics is highly influenced by the configuration of fire sources, especially by spacing between fires. Two effects can be expected when multiple fires are located sufficiently close to each other. First, burning intensity becomes stronger due to additional heat feedback from neighboring flames. Second, deterioration of combustion efficiency occurs at the inner side of multiple fires because the oxygen supply is hindered by outer flames. These opposite reactions take place at the same time and lead to a nonmonotonic dependency of burning intensity on gap spacing between fires. This trend has been experimentally studied using multiple hydrocarbon fuel pools [24–26]. The global burning rate measured based on burn-out time of each pool exhibited the increasing and decreasing trend with decreasing spacing [25]. In multiple solid fires using wood cribs, however, the intensified heat release rate was reported with increasing spacing [27,28]. It is presumed that the increased air entrainment through wider spacing played a role of intensifying the multiple fires in this case. However, the intensity of multiple fires is to decay at a certain spacing as the flame interaction becomes weak and flame separation occurs.

In spite of the in-depth research above, there still exists a necessity to study the thermal interaction between multiple heat sources and its influence on heat intensity. In a numerical simulation, it was found that there is a minimum energy required for the ignition of fuel substrate with increasing heat input, same as non-monotonic behavior of burning intensity in multiple pool fires [29]. Considering the competing reaction between heat feedback enhancement and air restriction rate in multiple fires, it is worth studying this mechanism on firebrand problem as well. Furthermore, there are relatively few research studying multiple solid fires available. This is mainly due to difficulties for combustion of solid fuels to reach steady state. This work attempts to investigate the thermal interaction between multiple flaming wooden cubes by varying their spatial distribution. The burning process of multiple wood samples is also the production process of firebrands prior to depositing them on a fuel substrate which will be performed in the future study. The goal of this study is to investigate the global and local burning behavior of a group of wood samples depending on different spatial distributions of fires and the thermal status of firebrands at the end of the flaming process.

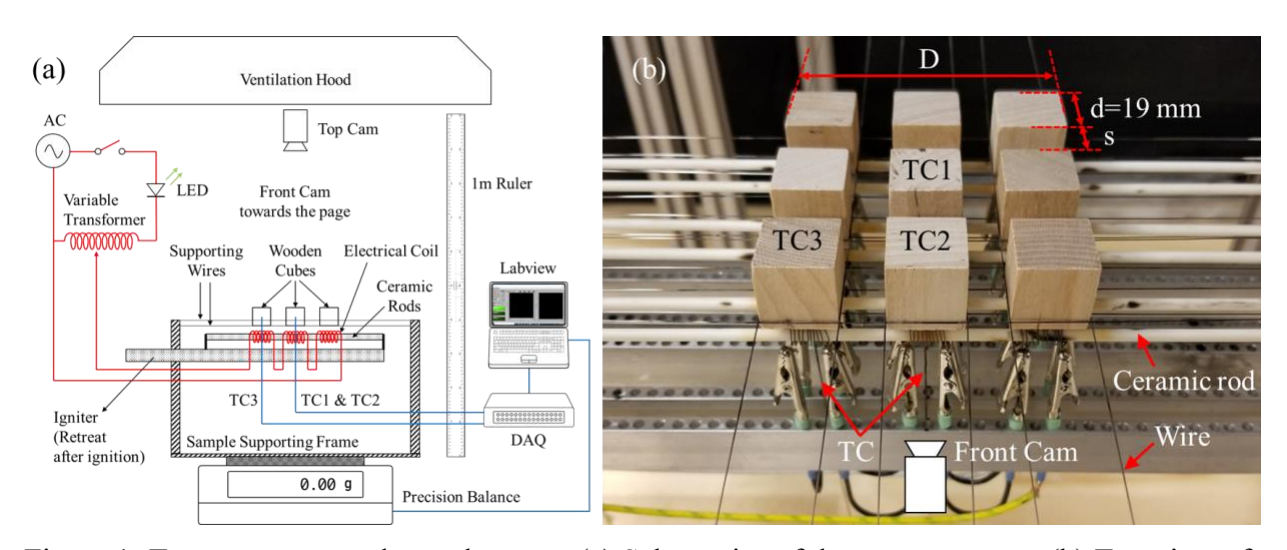


Figure 1: Test apparatus and sample setup. (a) Schematics of the test apparatus. (b) Top view of the sample arrangement and thermocouple locations. TC: Thermocouple.

2. Experimental Setup

A new experimental apparatus was designed and constructed for this study. The apparatus, as shown in Figure 1a, consists of three major components, wooden cube samples, sample supporting frame, and igniter. The entire apparatus was situated under a ventilation hood and surrounded by a hazard screen to mitigate flow disturbance from ambient air and to prevent burning debris from escaping.

Untreated 19.05 mm (3/4") birch wooden cubes [30] were used as solid samples in this study. Sample cubes were fully dried at 377 K (104 °C) in an oven for at least 12 hours prior to each test to remove moisture content. Mass of the sample cubes was monitored during the drying process and was observed to become stable in the initial 80 minutes. After fully dried, nine wood samples were arranged on supporting wires in a square pattern as shown in Figure 1b. The gap spacing (s) between the cube samples varied between 0 and 30 mm in different tests. In addition, burning of a single cube (positioned in the center) was also tested as a reference for comparisons.

The sample supporting frame was constructed using black anodized and matt-black painted aluminum to minimize the radiation reflection during the experiments. The frame has an overall dimension of 380 mm by 380 mm cross-section and is 300 mm in height. Stainless-steel supporting wires were mounted horizontally on the top surface of the frame through drilled holes with 5 mm intervals. These wires control the spacing and hold the cube samples in place during the burning process. The diameter of the wires was chosen after a series of trial tests. It was determined that 0.36 mm (0.014") was the minimum diameter for the wires to survive the fires in this study. One end of the wire was fixed on a side plate of the supporting frame and the other end of the wire was hooked to the frame using a spring. This is to maintain the wire tension when the wire was subject to heat from the fires.

The ignitors were made of electrical coils wrapped around ceramic rods (3.175 mm in diameter, see Figure 1). Each coil was fabricated by rounding TEMCO Kanthal A-1 29AWG wires 10 times on a 10-32 threaded rod and has a resistance of 3.9 ± 0.2 ohms. During the heating and ignition process, a pair of coils, positioned 5 mm underneath each cube sample, were powered at 3.5 amps for 30 seconds to ignite the sample. This heating duration ensures ignition and the establishment

of self-sustained flame for each of the wooden samples. After that, the ignitors retreated from the wooden cubes. The samples were left to burn to completion.

Two DSLR cameras (Canon T3i) were used to record the entire burning process (1,920 × 1,080 pixels at 30 frames per second), one from the front and one from the top. The front-view camera was manually fixed to the same settings in all tests (ISO: 1600, shutter speed: 1/60, aperture: F4.5). This facilitates the comparison of flame shape and height between different frames and between different tests. The top camera was set to auto-adjusted ISO to capture clear images of both bright flaming and dim smoldering stages of the burning process (ISO: auto, shuttle speed: 1/40, aperture: F1.8). A 1-meter ruler was positioned vertically on the mid-plane of the sample arrangement and next to the sample supporting frame. Calibrations were performed prior to the tests and it was determined that the pixel resolution is 0.29 mm/pixel. To eliminate the background noise of the video frames, a black curtain was installed behind the experimental setup. It covered the entire camera field of view. All experiments were performed in a dark room. A small green LED light was turned on while the igniter was on for time synchronization of the two camera recording.

K-type thermocouples with 0.508 mm (0.02") bead diameter were used to measure temperature of the wooden cubes at three selected sample locations (Figure 1b). The thermocouples were inserted to the cube center through a drilled hole from the bottom side to avoid contact with the flame. A precision balance (A&D GX-8K) with 0.01 g accuracy was also used to monitor the global mass loss of the samples during the experiments. The temperature and mass data were recorded at 2.1 Hz and 2.9 Hz respectively.

An image processing code was developed to extract the flame shape from the front-view camera images. The contrast of a RGB image was enhanced before image processing to remove the blur created by luminous flames. After that, the code converts the RGB images to grayscale and then binary images to determine the flame edge. Example RGB and transformed binary images are shown in Figure 2. The extracted flame edge is superimposed in both images (green lines in Figure 2). In this work, flame height was defined as the distance from top surface of sample cubes to the highest point of the flame (see Figure 2).

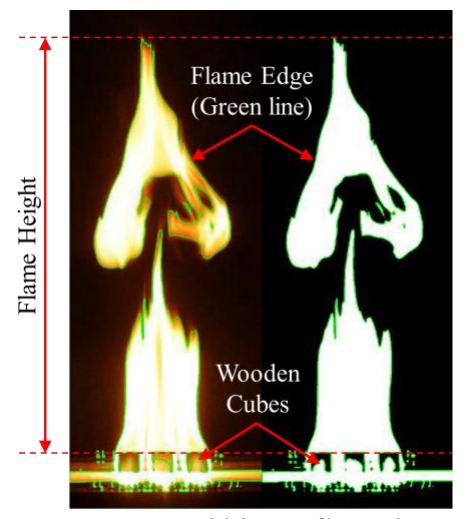


Figure 2: RGB and binary flame images

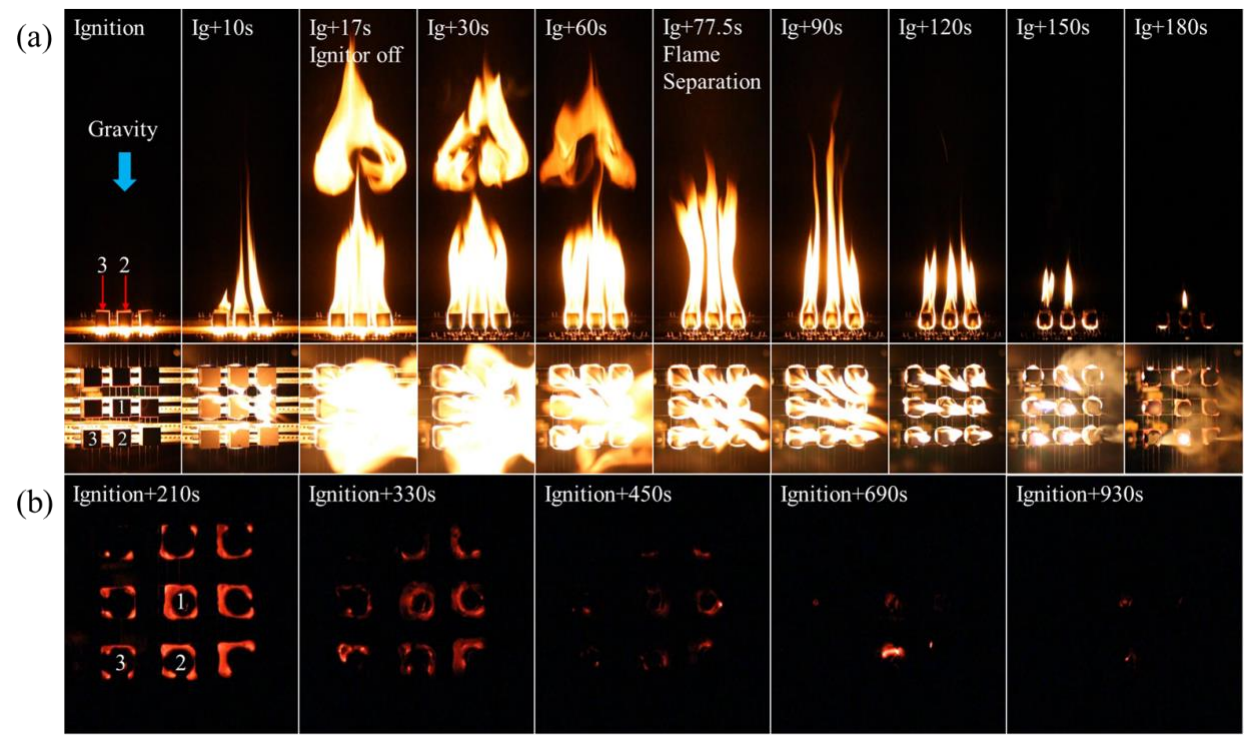


Figure 3: The sequential (a) flaming and (b) smoldering images. s = 10 mm.

3. Results and Discussion

3.1 Burning process of a group of solid fuels

Typical burning process observed in this work is demonstrated using a representative case with s=10 mm. Figure 3a shows the front and top view images of the flaming process of the nine wooden cubes. Note that t=0 is defined as the instance the ignitor is on. In this representative case, the flaming process lasted for ~206 s after ignition occurs. After flames extinguished, the top-view images (Figure 3b) show that the smoldering combustion continued for another 833 s. Note that the top view camera was positioned on top of the sample setup with a slightly tilted angle to protect the camera from direct impingement of fire plume and smoke.

Figure 3a shows that shortly after ignition, flames from wooden samples merged and formed a single large turbulent flame. Typical pulsing of fire plume was observed. The pulsing frequency was ~ 7.2 Hz, which is closed to the predicted value for pool fires with a similar dimension (5.3 Hz for D = 80 mm [31]). Flame separation occurred at 90.0 s. After that, flames became weaker and flame oscillation was mitigated. Note that the flame merging phenomenon was only observed for cases with s ≤ 10 mm. For gap sizes larger than 10 mm, flames from individual wooden cubes were observed to be always separated and the flame heights were generally shorter.

Also note that, in a short period of time (28 s) before flame extinction, flames from individual wooden sample would extinguish momentarily and re-ignite. This re-ignition was observed at all spacing except for s = 2.5 and 5 mm. The re-ignition repeated multiple times for individual samples before complete extinction occurred for all nine samples. It is suspected that an individual flame extinction occurred due to decrease in fuel volatile generation when the solid burning rate is low. But the volatile was re-ignited by heat from adjacent flames. Eventually, the flame completely extinguished (218.6 s) and the combustion process transited from flaming to smoldering.

In Figure 3b, glowing of the nine samples was clearly visible in the early stage of the smoldering process but it gradually weakened as charred cubes turned into ashes. During smoldering, cracks developed on charred sample surfaces, leading to partially or completely split of a sample in some cases. Ashes also collapsed when it failed to sustain its weight. These structural changes kept exposing new charred surfaces to the air and sustained smoldering until the combustible of the sample fully consumed.

Figure 4 presents the experimental measurements of the representative case (shown in Figure 3). Figure 4a shows the temperature readings (T) up to 1,100 seconds. Figure 4b focuses on the flaming process and shows the sample mass loss rate (dm/dt), remaining mass fraction (m/m0), and flame height (Z_f) up to t \sim 300 s. In this representative case, major observed burning events include: I) ignition, II) flame merging, III) flame separation, IV) flame extinction, and V) smoldering extinction. These burning events are marked in all plots in Figure 4.

Figure 4a shows that sample temperatures started rising once the ignitors were on (at t=0). Ignition occurred at ~ 12.5 s. After the ignitors were removed (t=29.5 s), the flame continued to heat up the samples at an approximately constant rate. For all three thermocouple locations, steep temperature increase was observed at ~ 670 K. This sharp increase in temperature was also observed in previous isothermal pyrolysis experiments of wooden samples in similar shape and size of those in this study [32]. This temperature spike is attributed to exothermic char formation process occurring after endothermic cellulose decomposition and volatiles generation [33]. The exothermic reaction provides heat, in addition to the flame heat feedback, to further increase the sample temperature. This exothermic smoldering combustion increased the sample temperature slightly even after the flame extinction occurred (t=218.6 s). The sample temperatures remained at 750-800K until the smoldering combustion ceased (t=1020.9 s)

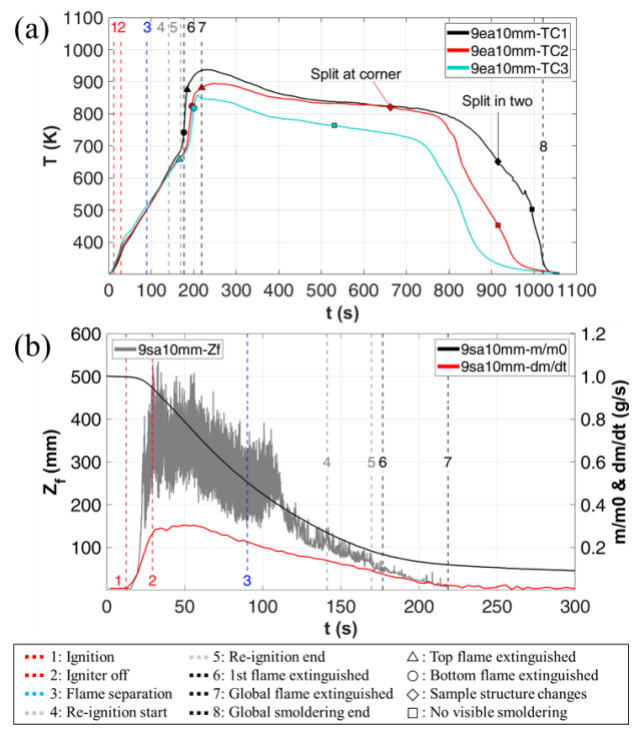


Figure 4: (a) Temperature of the wooden samples. (b) Flame height, sample remaining mass fraction, and mass loss rate. s = 10 mm.

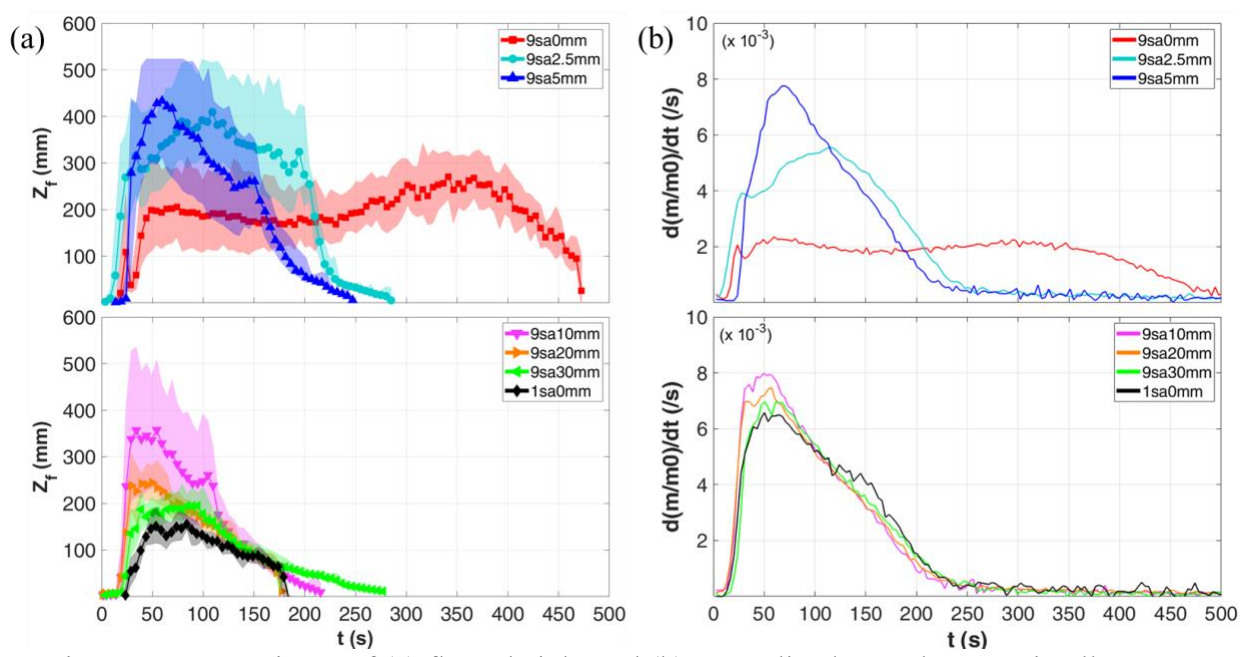


Figure 5: Comparisons of (a) flame height and (b) normalized mass loss rate in all cases.

Note that the temperature readings in Figure 4a did not show plateaus or a lower heating rate during sample endothermic decomposition process as seen in previous work (e.g., [32]). It is presumed that the degradation of various components of the wooden samples overlap with each other due to a fast heating, and consequently the endothermic cellulose decomposition process is clouded by the exothermic reaction [34].

The sample mass loss rate and flame height in Figure 4b increase sharply at ignition. They continue to rise up to peak values, remain at the peak values for a short period of time, and then decay as the sample burns out slowly. Note that when flame separation occurs (at \sim 90.0 s), a slight increase in flame height is observed. Sample mass loss rate became negligible when extinction of the flaming combustion occurred.

3.2 The spacing effects on flame height and mass loss rate

Figure 5 compares flame heights (Z_f) and normalized mass loss rates (d(m/m0)/dt) between different cases. For ease of reading, flame height was time-averaged every 5 seconds and its fluctuations was denoted as shaded area. Similar evolutions of the flame height and the mass loss rate are observed at all spacing except for s=0. Flame images are also compared in Figure 6. In these images, the mass loss rates reach peak values in each case.

At s = 0, flames merged as a large single fire at all times until extinction. The merging flame was observed to be weaker and shorter than that of all other spacing. The evolution of the mass loss rate (Figure 5b) also suggests that the sample burning process, while lasting longer, was significantly less intense. Multiple reasons can contribute to this. First, at s = 0, side surfaces between samples were not exposed to the flame at early stage of flaming. This results in a smaller effective sample pyrolysis area and a lower solid burning rate. Insufficient air supply to the center of the merging flame also contributed to a weaker flame. While flaming, a fuel rich zone appears at the center of the flame near the sample top surfaces (Figure 6). The fuel rich zone contains little oxygen and is of lower temperature than the outer flames [35]. The presence of the fuel rich zone

also implies that the sample at the center receive least heat input and has the lowest solid burning rate compared to the other samples.

Another observation for the case with s=0 is that the flame height and the sample mass loss rate both have a second peak (at ~ 350 s in Figure 5). This is because as the samples burned, sample volume became smaller and small gaps were created between samples. This exposed sample side surfaces to the flame and allowed oxygen penetrate to the flame center, improving the combustion efficiency.

Figure 7 further compares the flame height and mass loss rate quantitatively between different cases. Maximum mass loss rate was deduced by averaging the data in 10-second windows. Averaged flame heights were also calculated in the same 10 second. The error bars in Figure 7 denote the differences between repetitive tests.

When gap spacing decreases from 30 mm to 10 mm, both flame height and mass loss rate increase. Compared with the single sample case, all these cases have a higher mass loss rate. This indicates that flames from adjacent samples enhance the heat feedback to the samples through radiation and convection. This thermal interaction between adjacent flames and the resulting enhanced solid burning rate contribute to the increased flame heights when the gap spacing decreases.

When gap spacing further decreases to $s \le 5$ mm, the flame suffers from oxygen deficiency. Notice that compared to s = 10 mm, cases of s = 2.5 and 5 mm have greater flame heights but smaller mass loss rates The reducing amount of air entrainment through the gaps between the samples (not only from the sides but also from the bottom) can lead to a longer flame at smaller gap spacing. Flame height has been shown to be dependent on air entrainment rate [36]. Longer flame allows more air to be entrained into the combustion zone. Hence, flame typically becomes longer in air restricted environments, such as walls or nearby corners [37,38]. As described earlier, the center region of the flame is lifted above the sample surface (see Figure 6) and flame temperature may also be lower due to local fuel rich condition. This results in a decrease of heat input to the sample surface and a reduced solid burning rate as the gap spacing decreases.

The combined effects of thermal enhancement and oxygen depletion lead to a critical spacing (s = 10 mm) for maximum burning intensity as shown in Figure 7. Above this critical spacing, burning of multiple solid samples is highly affected by heat feedback enhancement received from other flames. Below the critical spacing, the combustion is under-ventilated and the amount of air entrainment plays a major role in the burning process. This phenomenon is similar to previous multiple pool fire experiments [24].

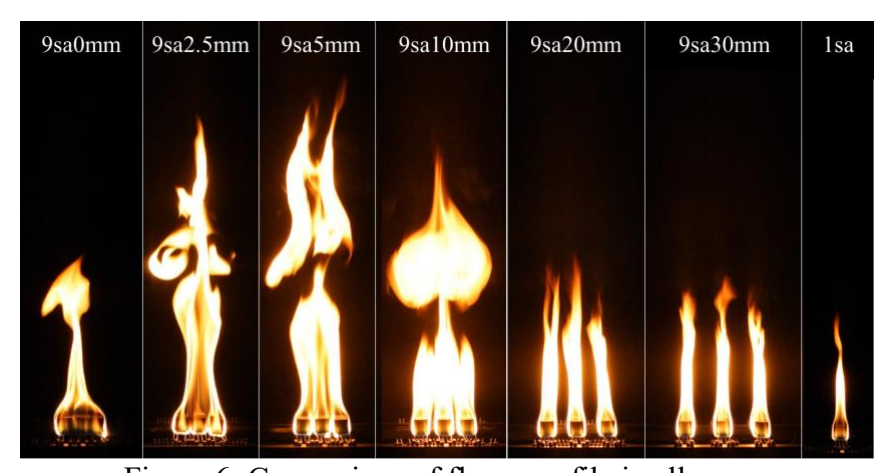


Figure 6: Comparison of flame profile in all cases.

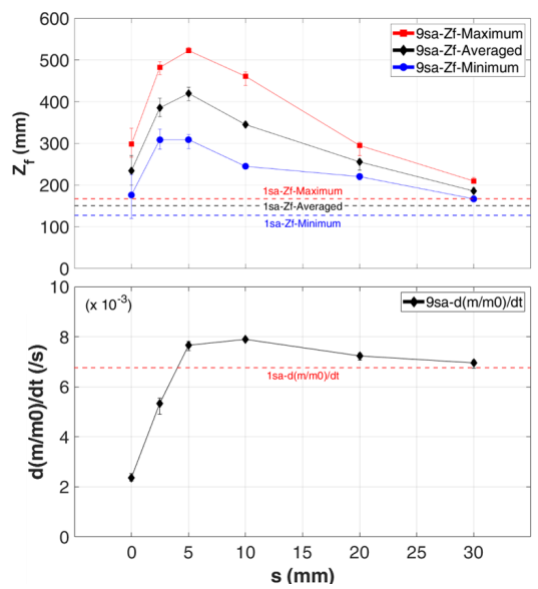


Figure 7: Maximum normalized mass loss rate and flame height for different sample separation distances.

3.3 The spacing effects on the temperature

Temperatures of the center sample (TC 1 in Figure 1) in different tests are compared in Figure 8. Variations between repetitive tests are marked at selected time instances using symbols with error bars. Note that, while not shown here, temperature evolutions at TC2 and TC3 locations are qualitatively similar to that shown in Figure 8.

In all cases, after the ignitor is off, sample temperature first increases with an approximately constant rate and then rises sharply due to exothermic decomposition to char as described earlier. It is shown that the peak temperature (during the exothermic decomposition) decreases monotonically with increasing spacing (except for a slight increase from 0 to 2.5 mm spacing). Similar to enhanced heat feedback from adjacent flames, thermal interactions between solid samples in close proximity during the exothermic decomposition also intensify the solid burning process.

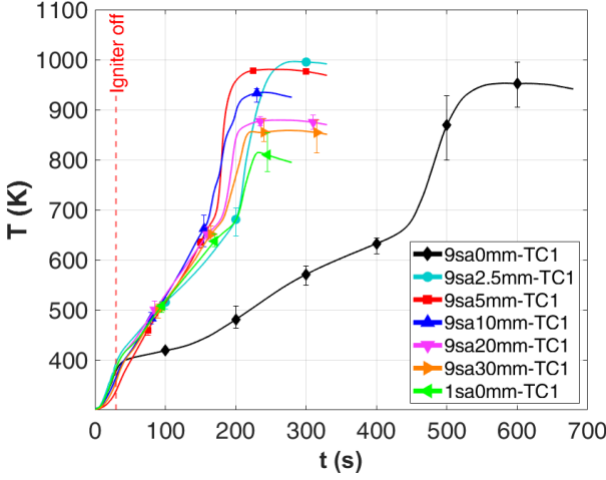


Figure 8: Comparisons of sample temperature evolution (TC1 readings) between different gap spacing.

Sub Topic: Fire Research

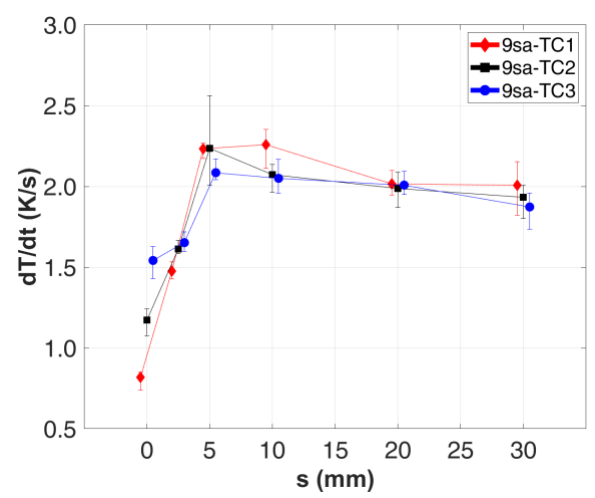


Figure 9: Sample heating rates during flaming combustion at all three thermocouple locations.

Heating rates during the flaming process were calculated over temperature range between 423 and 623 K (150 and 350 °C) using least squares method. The results are compared between different cases in Figure 8. Error bars denote the variation between repetitive tests. For ease of reading, data for TC1 and TC3 are slightly shifted left and right respectively (by 0.5 mm to avoid overlapping of the error bars) in the plot.

Similar to the mass loss rate, sample heating rate during flaming combustion, exhibits a non-monotonic dependency on the gap spacing. Among the three sample locations, sample at the center (TC1) is most influenced by the gap spacing and the corner sample (TC3) shows least variations between different cases. At small spacing ($s \le 2.5 \text{ mm}$), heating rates at all three locations are lower than that of single sample case. Furthermore, center sample has the lowest and corner sample has the highest heating rate. These once again suggest that the gaseous combustion suffers from oxygen deficiency and the heat feedback to the solid samples is reduced at these small gap spacing. In addition, at s = 0, sample side surfaces were facing each other and were not exposed to flames at the early stage of flaming, further reducing the heat received by the sample.

When the gap spacing is above s = 5 mm, the heating rates in all cases are higher than that of single sample case. In addition, the heating rate of the center sample (TC1) is larger than that of the side (TC2) and corner (TC3) samples. This once again demonstrates that the enhanced heat feedback is due to the thermal interactions between adjacent flames. The heating rates at the side and corner samples were found to be similar to each other in this 3 by 3 fuel pattern with gap spacing considered. When $s \ge 20$ mm, flames from individual samples never merge and the heating rate gradually decreases to the single-sample result when spacing increases.

3.4 Flame height correlation

Dimensionless flame height is plotted against dimensionless heat release rate in Figure 10. The dimensionless heat release rate is defined as follows [39].

$$Q_D^* = \frac{\dot{m}_f \Delta H_c}{\rho_0 c_p T_0 \sqrt{g} L_c^{5/2}} \tag{1}$$

Here ρ_0 , c_p , T_0 , and g are the ambient air density, specific heat, ambient temperature, and the gravitational acceleration, respectively. \dot{m}_f and ΔH_c are the mass loss rate and the heat of

combustion of the solid fuel (16.09 kJ/g for cellulose). L_c is the characteristic length. When the fire merges, the total edge length D (see Figure 1b) is used ($L_c = D$). When the fire separates, the edge length of the wooden sample d is used ($L_c = d$). Note that in each case, transient data from the flaming process is used.

Correlations deduced by Heskestad [40] and Quintiere and Grove [39] for axisymmetric fire source are included in Figure 10. These correlations are as follows.

$$Q_D^* = 0.0059 \frac{\psi^{3/2}}{1 - X_r} \sqrt{\left(\frac{z_f}{L_c}\right)} \left(1 + 2(0.179) \left(\frac{z_f}{L_c}\right)\right)^2$$
 (2)

$$Q_D^* = \left(\frac{z_f/L_c + 1.02}{15.6}\right)^{5/2} \left(\frac{\psi}{1 - X_r}\right)^{3/2} \tag{3}$$

where X_r is the flame radiant loss (= 0.3 in the plot) and ψ is defined below.

$$\psi = \frac{(1 - X_r)(\Delta H_a)}{c_p T_0} \tag{4}$$

 ΔH_a is the heat of combustion per unit mass of air consumed (2.91 kJ/g for methane).

For cases where combustion is under-ventilated (s = 0 and 2.5 mm), flame heights are higher compared to other cases at the same heat release rate. For cases with s \geq 5 mm, data from different states of the burning in each test and from different tests generally follows the previous correlations.

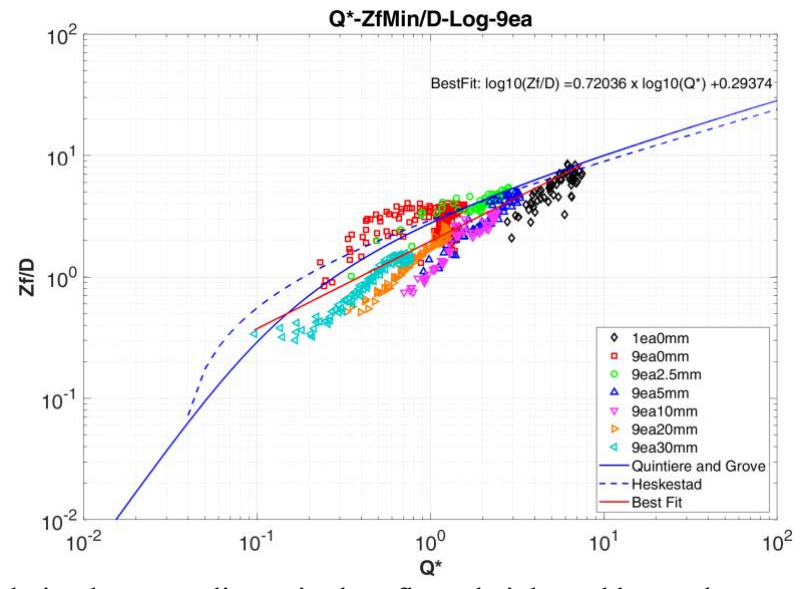


Figure 10: Correlation between dimensionless flame height and heat release rate transient data.

4. Conclusions

A series of experiments were performed to study the effect of spatial distribution on the burning characteristics of 3 by 3 multiple solid fires without a floor using a newly built apparatus. Small birch wooden cube samples were fully dried in this study. The gap spacing between samples (s) was carefully adjusted from 0 to 30 mm. The transient burning behaviors of the samples were shown to depend on the sample arrangement.

It was found that the global mass loss rate and flame height change non-monotonically when spacing varies. Maximum mass loss rate occurs at s = 10 mm for this specific set of experiments. At spacing larger than this critical spacing, mass loss rate and flame length increase when spacing decreases. This is because samples received enhances heat feedback not only from its own flame but also from neighboring ones. At the critical spacing, it is observed that flames from the nine samples merged. Air entrainment became restricted to the inner flames. As a result, the sample at the center experienced oxygen deficiency and the flame lifted from the sample surface. Flame temperature is likely also lower. These result in a reduced heat input to the sample and decreased mass loss rate.

The temperature of the wooden samples is shown to be a good indicator of burning intensity of multiple solid fires. Typical pyrolysis behavior of biomass was observed and showed the exothermic reaction increased the temperature to the peak value. The center position of multiple fires exhibited the peak temperature as expected. A similar non-monotonic trend was confirmed in the analysis of heating rate. It was found that the sample at the center changed the most with varying spacing. At small spacing, the heat feedback to the sample was smaller than the single sample result. Also the outer samples received the stronger flame heat feedback. As the spacing larger than the critical spacing, the sample at the center received the highest flame heat feedback. The outer samples experience more heat loss due to weak heat feedback enhancement and convective cooling.

The burning process of multiple fires was affected by spatial distribution effects as seen in the experiments of multiple pool fires. However, the strong heat of combustion may contribute to the higher heat feedback from a merged flame. Also multiple solid fires were influenced by the actual burning surface area unlike the multiple pool fires. Other geometrical factors such as height of samples may cause the different burning characteristics. These factors need to be taken into account in future studies.

Finally, the flame height was correlated to the burning rate. It was shown that the dimensionless heat release rate has a linear relationship with the flame height.

5. Acknowledgements

This research was funded by the National Science Foundation under grant number CBET-1836428.

6. References

- [1] U.S. Global Change Research Program, Wuebbles, D. J., Fahey, D. W., Hibbard, K. A., Dokken, D. J., Stewart, B. C., and Maycock, T. K. *Climate Science Special Report: Fourth National Climate Assessment, Volume I.* U.S. Global Change Research Program, 2017.
- [2] Goss, M., Swain, D. L., Abatzoglou, J. T., Sarhadi, A., Kolden, C. A., Williams, A. P., and Diffenbaugh, N. S. "Climate Change Is Increasing the Likelihood of Extreme

- Autumn Wildfire Conditions across California." *Environmental Research Letters*, Vol. 15, No. 9, 2020, p. 094016. https://doi.org/10.1088/1748-9326/ab83a7.
- [3] State of the Climate: Global Climate Report for Annual 2020. NOAA National Centers for Environmental Information. https://www.ncdc.noaa.gov/.
- [4] Top 20 Largest California Wildfires. *Cal Fire*. https://www.fire.ca.gov/stats-events/.
- [5] Maranghides, A., Link, E., Mell, W. "Ruddy," Hawks, S., Wilson, M., Brewer, W., Brown, C., Vihnaneck, B., and Walton, W. D. *A Case Study of the Camp Fire Fire Progression Timeline*. Publication NIST TN 2135. National Institute of Standards and Technology, Gaithersburg, MD, 2021, p. NIST TN 2135.
- [6] Caton, S. E., Hakes, R. S. P., Gorham, D. J., Zhou, A., and Gollner, M. J. "Review of Pathways for Building Fire Spread in the Wildland Urban Interface Part I: Exposure Conditions." *Fire Technology*, Vol. 53, No. 2, 2017, pp. 429–473. https://doi.org/10.1007/s10694-016-0589-z.
- [7] Fernandez-Pello, A. C. "Wildland Fire Spot Ignition by Sparks and Firebrands." *Fire Safety Journal*, Vol. 91, 2017, pp. 2–10. https://doi.org/10.1016/j.firesaf.2017.04.040.
- [8] Manzello, S. L., Suzuki, S., Gollner, M. J., and Fernandez-Pello, A. C. "Role of Firebrand Combustion in Large Outdoor Fire Spread." *Progress in Energy and Combustion Science*, Vol. 76, 2020, p. 100801. https://doi.org/10.1016/j.pecs.2019.100801.
- [9] Suzuki, S., Brown, A., Manzello, S. L., Suzuki, J., and Hayashi, Y. "Firebrands Generated from a Full-Scale Structure Burning under Well-Controlled Laboratory Conditions." *Fire Safety Journal*, Vol. 63, 2014, pp. 43–51. https://doi.org/10.1016/j.firesaf.2013.11.008.
- [10] Suzuki, S., and Manzello, S. L. "Firebrand Production from Building Components Fitted with Siding Treatments." *Fire Safety Journal*, Vol. 80, 2016, pp. 64–70. https://doi.org/10.1016/j.firesaf.2016.01.004.
- [11] Suzuki, S., Manzello, S. L., and Hayashi, Y. "The Size and Mass Distribution of Firebrands Collected from Ignited Building Components Exposed to Wind." *Proceedings of the Combustion Institute*, Vol. 34, No. 2, 2013, pp. 2479–2485. https://doi.org/10.1016/j.proci.2012.06.061.
- [12] Manzello, S. L., Park, S.-H., Suzuki, S., Shields, J. R., and Hayashi, Y. "Experimental Investigation of Structure Vulnerabilities to Firebrand Showers." *Fire Safety Journal*, Vol. 46, No. 8, 2011, pp. 568–578. https://doi.org/10.1016/j.firesaf.2011.09.003.
- [13] Manzello, S. L., and Suzuki, S. "Experimental Investigation of Wood Decking Assemblies Exposed to Firebrand Showers." *Fire Safety Journal*, Vol. 92, 2017, pp. 122–131. https://doi.org/10.1016/j.firesaf.2017.05.019.
- [14] Manzello, S. L., Suzuki, S., and Hayashi, Y. "Exposing Siding Treatments, Walls Fitted with Eaves, and Glazing Assemblies to Firebrand Showers." *Fire Safety Journal*, Vol. 50, 2012, pp. 25–34. https://doi.org/10.1016/j.firesaf.2012.01.006.
- [15] Manzello, S. L., Hayashi, Y., Yoneki, T., and Yamamoto, Y. "Quantifying the Vulnerabilities of Ceramic Tile Roofing Assemblies to Ignition during a Firebrand Attack." *Fire Safety Journal*, Vol. 45, No. 1, 2010, pp. 35–43. https://doi.org/10.1016/j.firesaf.2009.09.002.
- [16] Suzuki, S., Nii, D., and Manzello, S. L. "The Performance of Wood and Tile Roofing Assemblies Exposed to Continuous Firebrand Assault: Wood and Tile Roofing

- Assemblies Exposed to Firebrand Showers." *Fire and Materials*, Vol. 41, No. 1, 2017, pp. 84–96. https://doi.org/10.1002/fam.2372.
- [17] Suzuki, S., Manzello, S. L., Kagiya, K., Suzuki, J., and Hayashi, Y. "Ignition of Mulch Beds Exposed to Continuous Wind-Driven Firebrand Showers." *Fire Technology*, Vol. 51, No. 4, 2015, pp. 905–922. https://doi.org/10.1007/s10694-014-0425-2.
- [18] Manzello, S. L., Suzuki, S., and Nii, D. "Full-Scale Experimental Investigation to Quantify Building Component Ignition Vulnerability from Mulch Beds Attacked by Firebrand Showers." *Fire Technology*, Vol. 53, No. 2, 2017, pp. 535–551. https://doi.org/10.1007/s10694-015-0537-3.
- [19] Salehizadeh, H., Hakes, R. S. P., and Gollner, M. J. "Critical Ignition Conditions of Wood by Cylindrical Firebrands." *Frontiers in Mechanical Engineering*, Vol. 7, 2021, p. 630324. https://doi.org/10.3389/fmech.2021.630324.
- [20] Tao, Z., Bathras, B., Kwon, B., Biallas, B., Gollner, M. J., and Yang, R. "Effect of Firebrand Size and Geometry on Heating from a Smoldering Pile under Wind." *Fire Safety Journal*, 2020, p. 103031. https://doi.org/10.1016/j.firesaf.2020.103031.
- [21] Hakes, R. S. P., Salehizadeh, H., Weston-Dawkes, M. J., and Gollner, M. J. "Thermal Characterization of Firebrand Piles." *Fire Safety Journal*, Vol. 104, 2019, pp. 34–42. https://doi.org/10.1016/j.firesaf.2018.10.002.
- [22] Manzello, S. L., Cleary, T. G., Shields, J. R., Maranghides, A., Mell, W., and Yang, J. C. "Experimental Investigation of Firebrands: Generation and Ignition of Fuel Beds." *Fire Safety Journal*, Vol. 43, No. 3, 2008, pp. 226–233. https://doi.org/10.1016/j.firesaf.2006.06.010.
- [23] Manzello, S. L., Park, S.-H., and Cleary, T. G. "Investigation on the Ability of Glowing Firebrands Deposited within Crevices to Ignite Common Building Materials." *Fire Safety Journal*, Vol. 44, No. 6, 2009, pp. 894–900. https://doi.org/10.1016/j.firesaf.2009.05.001.
- [24] Liu, N., Liu, Q., Lozano, J. S., Shu, L., Zhang, L., Zhu, J., Deng, Z., and Satoh, K. "Global Burning Rate of Square Fire Arrays: Experimental Correlation and Interpretation." *Proceedings of the Combustion Institute*, 2009, p. 8.
- [25] Liu, N., Liu, Q., Lozano, J. S., Zhang, L., Deng, Z., Yao, B., Zhu, J., and Satoh, K. "Multiple Fire Interactions: A Further Investigation by Burning Rate Data of Square Fire Arrays." *Proceedings of the Combustion Institute*, Vol. 34, No. 2, 2013, pp. 2555–2564. https://doi.org/10.1016/j.proci.2012.06.098.
- [26] Jiao, Y., Gao, W., Liu, N., Lei, J., Xie, X., Zhang, L., and Tu, R. "Interpretation on Fire Interaction Mechanisms of Multiple Pool Fires." *Proceedings of the Combustion Institute*, Vol. 37, No. 3, 2019, pp. 3967–3974. https://doi.org/10.1016/j.proci.2018.06.049.
- [27] Kamikawa, D., Weng, W. G., Kagiya, K., Fukuda, Y., Mase, R., and Hasemi, Y. "Experimental Study of Merged Flames from Multifire Sources in Propane and Wood Crib Burners." *Combustion and Flame*, Vol. 142, Nos. 1–2, 2005, pp. 17–23. https://doi.org/10.1016/j.combustflame.2005.02.004.
- [28] Weng, W., Kamikawa, D., and Hasemi, Y. "Experimental Study on Merged Flame Characteristics from Multifire Sources with Wood Cribs." *Proceedings of the Combustion Institute*, Vol. 35, No. 3, 2015, pp. 2597–2606. https://doi.org/10.1016/j.proci.2014.05.112.
- [29] Liao, Y.-T. T., and T'ien, J. S. "A Numerical Simulation of Transient Ignition and Ignition Limit of a Composite Solid by a Localised Radiant Source." *Combustion Theory*

- *and Modelling*, Vol. 17, No. 6, 2013, pp. 1096–1124. https://doi.org/10.1080/13647830.2013.831486.
- [30] American Woodcrafters Supply. https://www.americanwoodcrafterssupply.com/. Accessed Feb. 5, 2021.
- [31] Cetegen, B. M., and Ahmed, T. A. "Experiments on the Periodic Instability of Buoyant Plumes and Pool Fires." *Combustion and Flame*, Vol. 93, Nos. 1–2, 1993, pp. 157–184. https://doi.org/10.1016/0010-2180(93)90090-P.
- [32] Atreya, A., Olszewski, P., Chen, Y., and Baum, H. R. "The Effect of Size, Shape and Pyrolysis Conditions on the Thermal Decomposition of Wood Particles and Firebrands." *International Journal of Heat and Mass Transfer*, Vol. 107, 2017, pp. 319–328. https://doi.org/10.1016/j.ijheatmasstransfer.2016.11.051.
- [33] Park, W. C., Atreya, A., and Baum, H. R. "Experimental and Theoretical Investigation of Heat and Mass Transfer Processes during Wood Pyrolysis." *Combustion and Flame*, Vol. 157, No. 3, 2010, pp. 481–494. https://doi.org/10.1016/j.combustflame.2009.10.006.
- [34] C.Di Blasi. "Modeling Chemical and Physical Processes of Wood and Biomass Pyrolysis." *Progress in Energy and Combustion Science*, Vol. 34, No. 1, 2008, pp. 47–90. https://doi.org/10.1016/j.pecs.2006.12.001.
- [35] Hamins, A., Kashiwagi, T., and Buch, R. Characteristics of Pool Fire Burning. In *Fire Resistance of Industrial Fluids* (G. Totten and J. Reichel, eds.), ASTM International, 100 Barr Harbor Drive, PO Box C700, West Conshohocken, PA 19428-2959, 1996, pp. 15-15–27.
- [36] James G. Quintiere. Fundamentals of Fire Phenomena. John Wiley & Sons, 2006.
- [37] Sugawa, O., Satoh, H., and Oka, Y. "Flame Height from Rectangular Fire Sources Considering Mixing Factor." *Fire Safety Science*, Vol. 3, 1991, pp. 435–444. https://doi.org/10.3801/IAFSS.FSS.3-435.
- [38] Poreh, M., and Garrad, G. "A Study of Wall and Corner Fire Plumes." *Fire Safety Journal*, 2000, p. 18.
- [39] Quintiere, J. G., and Grove, B. S. "A Unified Analysis for Fire Plumes." *Symposium (International) on Combustion*, Vol. 27, No. 2, 1998, pp. 2757–2766. https://doi.org/10.1016/S0082-0784(98)80132-X.
- [40] Heskestad, G. "A Reduced-Scale Mass Fire Experiment." 1991, p. 9.